International Journal on Science and Technology (IJSAT)
E-ISSN: 2229-7677 ● Website: www.ijsat.org ● Email: editor@ijsat.org

Experimental Investigation of Entirely Detached Growth in Vertical Directional Solidification and Crystallization Evolution

Dattatray Gadkari

Independent Researcher, Shree Yogesh Tower, Kora Kendra, Borivali (W), Mumbai 400092 India
Lead presenter: db.gadkari@gmail.com

Abstract

Vertical Directional Solidification (VDS) process produces entirely detached, diffusion-controlled crystallization of Sb-based III–V alloys, binary - InSb, GaSb, doped derivatives, ternary $In_{(1-X)}Ga_XSb$, and $In_{0.5}Ga_{0.5}Sb$ alloys under fully terrestrial conditions. Establishing a vapor-rich, pressure-compensated melt environment and the axial gradients (10–32 °C·cm^{-1}), by naturally suppresses buoyancy-driven flow and shear stress at the ampoule boundary. This creates a quasi-equilibrium vapor–melt–crystal domain where solute transport becomes overwhelmingly governed by thermodiffusion and diffusion, yielding a stable, thick diffusion boundary layer. VDS experimental results reveal uniform compositions ($\Delta x < 0.01$), insignificant segregation, and high structural perfection (FWHM 49–128 arcsec). Entire interface detachment attained across all compositions eliminates wall-induced perturbations and establishes the classical Concave → Planar → Convex meniscus alike crystallization obtained in space growth or in microgravity. Quantitative evaluation of thermal diffusion, diffusion fluxes, interface thermodynamics, and detachment parameters confirms repeats (~80 runs) of the transport physics of solidification. VDS results constitutes a dynamic terrestrial crystallization, enabling superior morphological stability, controlled solute redistribution, and exceptional crystalline quality.

Keywords: Vertical Directional Solidification (VDS); Sb-Based III–V Alloys; Entire Detachment; Thermodiffusion; Quasi-Microgravity; Diffusion-Controlled Growth;

1. Introduction

Producing high-quality single crystals of III–V semiconductors under terrestrial conditions is inherently constrained by the presence of buoyancy-driven convection, thermal asymmetry, solute boundary-layer instability, and strong interactions between the melt and the container wall. These limitations profoundly influence segregation, crystalline perfection, and interface morphology during melt growth of InSb, GaSb, and related ternary alloys (Akamatsu et al., 2025; Zhao et al., 2023). Conventional bulk growth methods operate in environments where gravitational forces inevitably induce convective recirculation and interfacial shear. As a consequence, these methods often yield non-uniform solute fields, faceting instabilities (Gransy et.al.2019), the wetting-driven defects, radial segregation, and elevated values for Growth Deviation (GD).

Microgravity experiments aboard the International Space Station (ISS) (Salgado Sánchez et.al. 2025) have revealed the dramatic improvement in morphological stability, compositional uniformity, and structural orderliness that emerges when convection is suppressed and diffusion dominates mass transport (Martínez et al. 2023; 2024; Regel et.al. 1999). Under microgravity, the Rayleigh number (Ra) approaches zero, allowing a thick, stable solute boundary layer to form adjacent to the crystal-melt interface. The growth front becomes smoother, segregation is minimized, and the interface curvature typically follows the Concave–Planar–Convex sequence for morphological stability theory (Alexandrov et.al 2024).

The environment naturally suppresses convective flow, establishes a quasi-equilibrium vapor–crystal–solute-melt system, and enables diffusion-dominated solute transport (Liu et.al. 2024; Shevtsova et.al. 2007). Unlike conventional methods (Ludwig et,al. 2022), the VDS system does not rely on large melt volumes or steep thermal gradients; instead, controlled vapor transport and mild gradients provide a stable environment in which the melt remains isolated from external hydrodynamic disturbances. These features promote conditions minimization of shear stress, suppression of buoyancy-driven instabilities (Ouadhan et.al. 2018), and stabilization of the crystal-melt interface. The VDS crystal growth process presents a promising approach to meeting these challenges, since 1994 (Gadkari et.al. 2012 to 2020), offers a fundamentally different approach to terrestrial crystal growth. Unlike classical melt-pulling techniques, VDS establishes a quasi-equilibrium vapor–melt–crystal environment inside a sealed ampoule. The combination of mild axial gradients, vapor-mediated pressure compensation, and controlled slow-freezing suppresses thermosolutal convection and minimizes hydrodynamic disturbances. Prior studies demonstrated partial detachment or localized wall separation in some systems (Regel et.al. 1999), but whole-ingot, contact-free growth under fully terrestrial conditions has remained an outstanding challenge.

In this work, VDS reliably produces entirely detached, diffusion-controlled crystallization of InSb, GaSb, doped derivatives, the ternary ($In_{(1-X)}Ga_XSb$), and $In_{0.5}Ga_{0.5}Sb$ alloys. Reveal how the vapor-driven pressure balance and stabilized meniscus inhibit melt wetting of the ampoule. How thermodiffusion governs solute redistribution in the absence of convection, and the interface curvature evolves contemporaneous in VDS experimental, analytical, and comparative evaluation. —including diffusion flux calculations, morphological stability interpretation, and GD quantification.

2. Experimental Procedure

2.1 VDS Furnace Configuration and Thermal Field

Crystal growth was performed using a vertically aligned VDS system consisting of a single-zone furnace and a sealed quartz ampoule of fixed geometry. The ampoule followed the standard VDS configuration previously established for III–V systems, the schematic process Fig-1a, true VDS process Fig-1b and thermal images inside vertical furnace Fig.1c. Where, the ampoule was having a cylindrical body, conical bottom to promote initial nucleation stability, and a planar vacuum-sealed top. This geometry minimizes radial thermal gradients and ensures symmetric heat transfer along the growth axis, enabling stable interface shaping and sustained detachment. The furnace produced a controlled axial temperature profile with three thermally distinct regions (PI, PII, PIII), as shown in Fig. 1(c). The centre of the furnace provided the melting temperature (PI high zone-850°C,), while progressively middle (PII 700°C zone) and lower temperatures (PIII 525°C zone) were maintained to establish solidification conditions. The axial gradient was maintained between 10 and 32 °C·cm^{-1}, consistent with the values used in microgravity

detached solidification experiments. Such mild gradients are critical for suppressing buoyancy-driven flow and maintaining a diffusion-dominated transport regime. The ampoule was placed inside a vertically aligned single zone furnace designed to generate a mild and controlled temperature gradient.

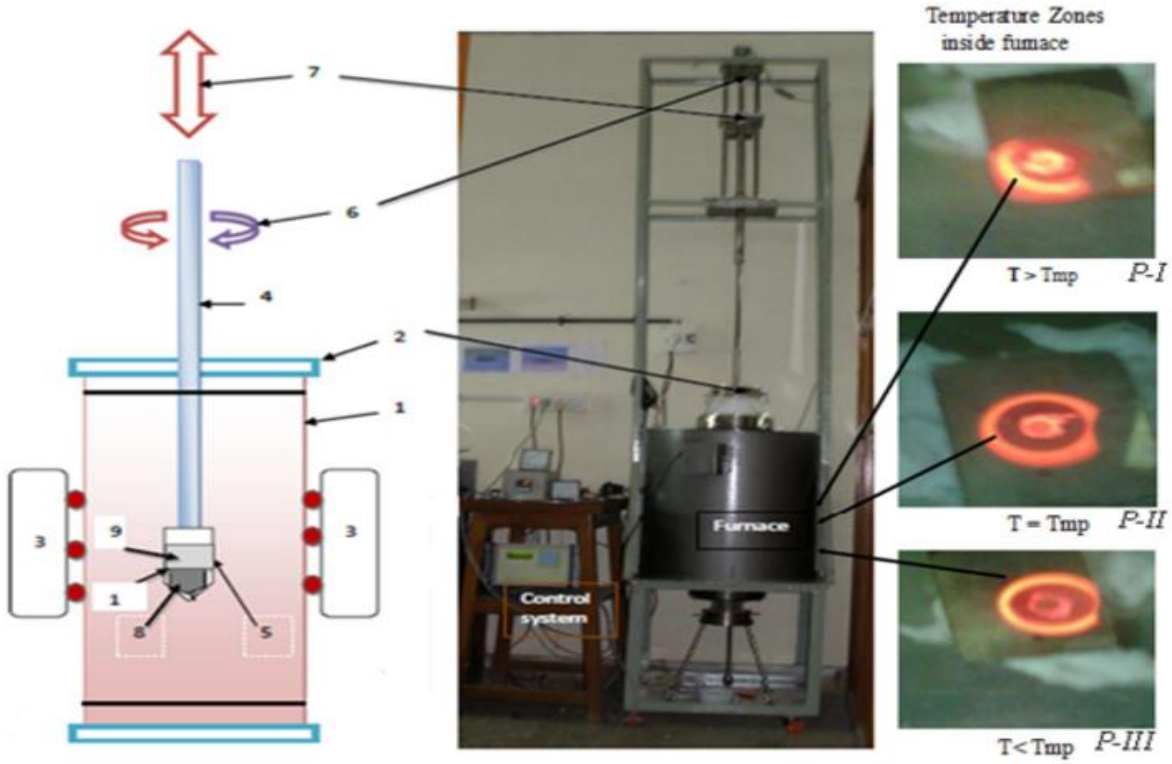

(a) (b) (c)

Fig.1 (a) schematic of the VDS process numbers represent: 1. Melt, 2. Wilson seal, 3. The vertical furnace profile, 4. Shaft, 5. Quartz ampoule, 6. Clock-anticlock rotation, 7. Up-down, 8. Detached crystal, 9. Vacuum, 10. quartz tube, (b) the photo of true VDS process, and (c) the thermal images inside vertical furnace.

Figure 1 provides visual confirmation of the physical environment that enables microgravity-equivalent transport during VDS crystal growth, Fig. 1(a) Schematic of VDS process shows the sealed quartz ampoule with a conical bottom and vacuum top. The vacuum region creates a low-density vapor-rich domain, which suppresses buoyancy convection and stabilizes the meniscus. The geometry ensures symmetrical heat flow, essential for maintaining a stable interface in diffusion-dominant regimes. Figure 1(b) real VDS growth experiment, demonstrates the operational alignment of the ampoule, showing no mechanical translation, unlike Bridgman or VGF. Solidification proceeds purely by controlled thermal modulation, which eliminating forced convection, and reinforcing microgravity equivalence. Figure 1(c) Thermal mapping of furnace shows three distinct thermal regions (PI, PII, PIII). PI is the melting zone; PII the intermediate zone; PIII the solidification zone. The gentle thermal gradient (10–32 °C.cm^{-1}) suppresses buoyancy-driven instabilities. This three-zone configuration produces the steady-state thermal symmetry reported in microgravity experiments. Importance is this figure establishes that the VDS setup

inherently produces a low-convection, diffusion-dominated environment, which is otherwise achievable only in microgravity.

The temperature gradient across the ampoule was maintained typically at 10-32^{0}C.cm^{-1} Fig. 2(a), and the unique seven steps growth profile Fig. 2(b) (Gadkari et.al 2012 to 2020) is sufficient to sustain vapor diffusion without generating significant thermal convection in the melt. This configuration progressively reduces melt superheat and enables a stable vapor–melt–crystal equilibrium. Solidification proceeded solely by controlled modulation of furnace temperature, allowing the crystal–melt interface to migrate through vapor-mediated equilibrium rather than forced transport. Figure 2 is the thermal engineering strategy that allows VDS to achieve stable diffusion-limited solidification, Fig. 2(a) axial temperature gradient. The gradient is mild (10–32 °C/cm), avoiding strong buoyancy flow, alike in microgravity experiments, which also rely on mild gradients because convection scales. A gentle gradient ensures that transport is dominated by Fick's law diffusion rather than convection. Figure 2(b) is Seven-Step VDS Growth Sequence shows reduction of melt superheat in steps, producing a controlled freezing front. Each step re-establishes vapor–melt equilibrium, preventing wetting or runaway supercooling. This slow freezing is essential for forming a thick diffusion boundary layer. Signifying the seven-step profile is a key reason into VDS process attains entire detachment and interface stability (space growth), despite being experiments done on Earth.

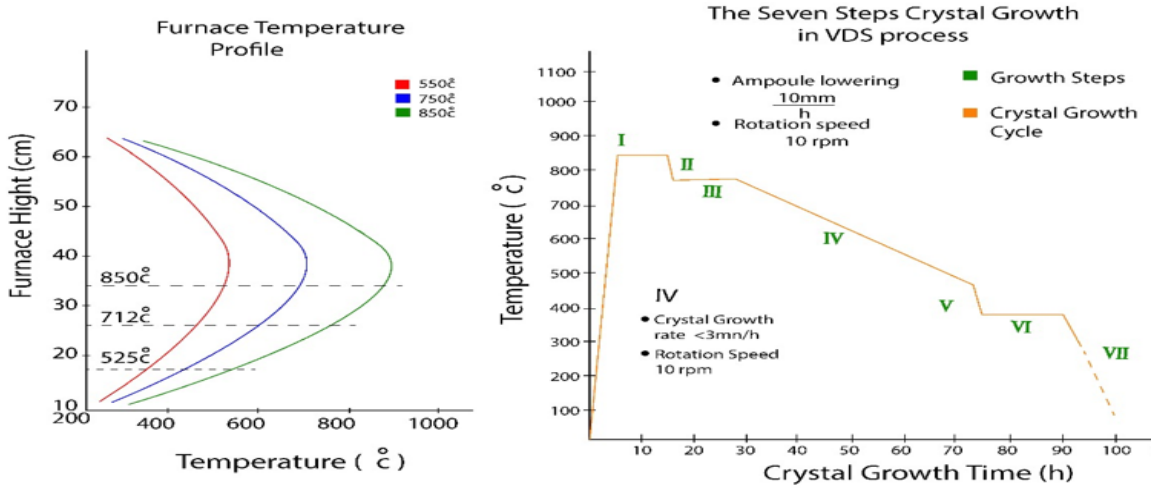

(a) (b)

Fig. 2 (a) the thermal profile of vertical furnace, and (b) the typical seven steps detached VDS growth process

2.3 Materials and Ampoule Preparation

Prior to sealing, the ampoules were chemically cleaned and heated under vacuum to remove surface contamination. The vacuum-sealed top created a low-density vapor region above the melt during growth. This region plays a central role in suppressing convection and maintaining detachment by reducing hydrostatic forces on the melt. High-purity (99.999%) elements—indium (In), gallium (Ga), and antimony (Sb)—were weighed in stoichiometric proportions for the preparation of InSb, GaSb, doped Sb-based alloys, the ternary ($In_{(1-X)}Ga_XSb$) and $In_{0.5}Ga_{0.5}Sb$. Table 1 (Sr. no. 1 to 4) summarizes the mass ratios, growth temperatures, dopant concentrations, thermal gradients, and resulting crystal dimensions. All samples were grown under vacuum and the high-purity argon atmospheres (0.025–0.028 MPa), ensuring

consistent vapor-pressure conditions across all experiments. The results of these two procedures were similar; the entire detachment was independent of filling of high-purity argon.

2.4 Conditions for Sustained Detachment

Figure 3(a) represents a schematic view and its thermal condition during VDS growth process, and are labelled different growth section, parameters, which are needed for growth. While, Fig. 3(b) is the picture of thermal field conditions into the vertical VDS furnace applied during growth, the colour corresponds to the different temperature fields (PI, PII, and PIII). However, the translation is downward direction against gravity, and the rotation is clock-wise or anti clock-wise. The black arrow in Fig. 3a is representing for vertical growth direction (not translation). A critical feature of VDS is its ability to maintain entire detachment between the growing crystal and the ampoule wall. Detachment arises from the interplay of vapor pressure at the upper region, meniscus curvature regulated by melt surface tension, mild axial gradients that promote uniform heat extraction, and non-wetting conditions between the III–V melt and quartz wall. As an enter detached solidification initiates contemporaneously by the i) vapor pressure exerts a counteracting force on the melt column, ii) reducing the effective hydrostatic pressure and iii) lowering the contact angle at the wall. The melt meniscus adopts a stable shape that prevents melt climb. This mechanism is analogous to the pressure-compensated melt behaviour observed in microgravity detached-solidification experiments, but here, experimentally (not serendipitously) achieved under terrestrial conditions.

Schematic and real thermal field inside the VDS furnace, Figure 3b clarifies how the furnace creates a stable thermal environment that minimizes convection. The thermal field surrounding the ampoule is nearly isothermal radially and graded only vertically. The vapor region buffers temperature fluctuations, preventing surface-tension-driven Marangoni flow. The downward translation direction and upward growth against gravity (apparent, not mechanical) show the effective movement of the crystal-melt interface and the variations of meniscus during controlled cooling. The combination of symmetric heating and vapor-pressure control produces a quasi-zero effective gravity at the crystal-melt interface and meniscus is very narrow region

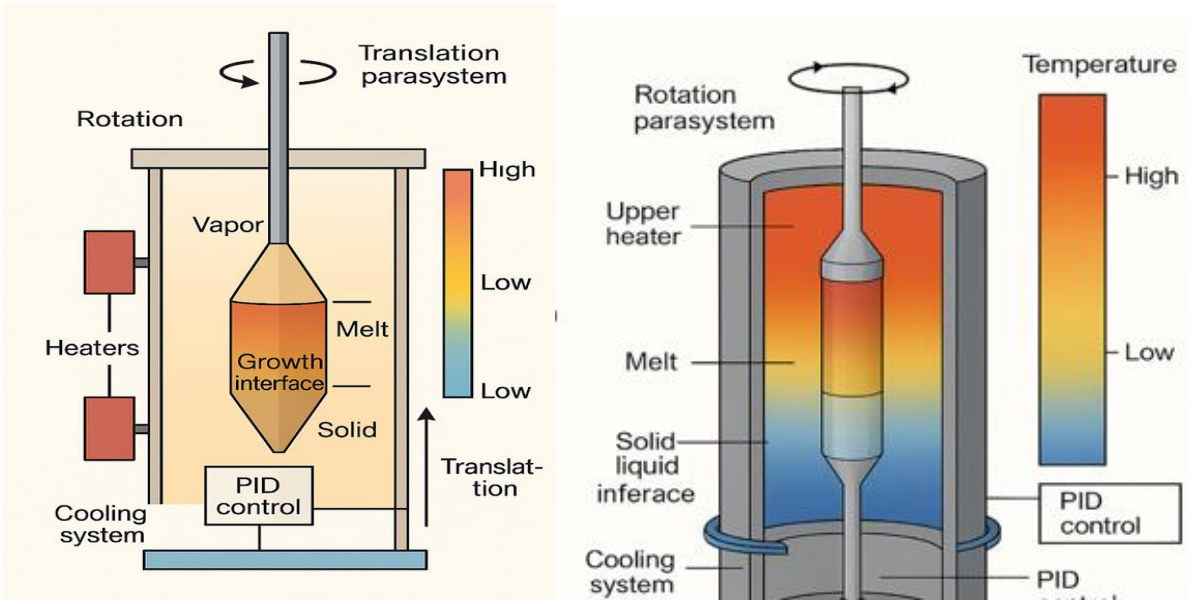

(a) (b)

Fig. 3 (a) the schematic VDS process, and (b) thermal fields inside a vertical furnace with ampoule inside the growth chamber (not as per scale), it is illustration of thermal field into VDS furnace.

of melt (detached region of mm size), because large melt above this in contact with ampoule wall. Importance is this figure provides evidence that the melt in VDS remains in a convection-free, diffusion-dominated state, alike microgravity conditions. Physical properties and growth conditions for all entire detached crystals: This table establishes the reproducibility across several categories of Sb-based alloys consistent success of entire detachment, low FWHM values indicating excellent structural order uniform pressure and thermal gradients across all runs wide composition range handled by VDS such as binary, doped derivative, ternary ($In_{(1-X)}Ga_XSb$), and $In_{0.5}Ga_{0.5}Sb$ crystals are given in Table 1. Scientific relevance, this proves that VDS process is not composition-sensitive and can reliably produce quasi-microgravity-equivalent crystallization across multiple III–V materials. The VDS experimental physical properties of InSb, GaSb, doped derivatives, ($In_{(1-X)}Ga_XSb$), and $In_{0.5}Ga_{0.5}Sb$ crystals are in Table 1.

Table 1, The black italic figures in brackets are number of growths runs for an entire detached crystals by VDS process on terrestrial conditions. Crystals grown - InSb:Bi ***(7)***, InSb:N ***(5),*** InSb:Se ***(3)***, GaSb:Mn ***(3)***, GaSb:Mg ***(2)***, and $Ga_{(1-X)}In_X$ Sb (8)**,** these crystals were grown by research scholars using VDS process since 1994 (Gadkari et.al. 2012 to 2020).

Sr No.	**Crystal ➡ Properties ⬇**	**InSb** ***(18)***	**InSb:Te** ***(4)***	**InSb:Bi** ***(4)***	**GaSb** ***(6)***	**GaSb: Te** ***(4)***	**GaSb:In** ***(4)***	**InSb:Ga** ***(5)***	**$In_{0.5}Ga_{0.5}Sb$** ***(10)***
1	**In (gms)**	9.68	9.72	9.57			0.66	2.62	2.98
2	**Ga(gms)**				20.95	6.8	3.61	4.76	11.21
3	**Sb(gms)**	10.24	10.28	10.37	37.16	11.2	7.0	11.12	4.82
4	**Dopant(gms)**		0.35 x	0.05		0.38 x	0.15%	0.25%	0.5%

			10^{-3}			10^{-3}			
5	**Set Temp (^{0}C)**	800	820	800	850	810	850	850	850
6	**Growth Temp (^{0}C)**	575	575	575	762	762	762	762	762
7	**Gradient (^{0}C. cm^{-1})**	10-32	10-32	10-32	10-32	10-32	10-32	10-32	10-32
8	**Up/Down rate (mm/h)**	5	5	2	5	5	5	5	3
9	**Rotation speed (rpm)**	10	10	10	10	10	10	10	10
10	**Cone angel (0^0)**	54	57	58	62	664	74	65	72
11	**Gap width (µm)**	69	112	73	95	128	139	151	145
12	**Crystal length (mm)**	62	60	58	75	66	42	52	49
13	**Crystal dia. (mm)**	12	12	10	22	18	10	14	12
14	**FWHM (arcsec)**	65	87	95	49	98	95	112	128
15	**Refl / Orient (Laue/Raman)**	220 /110	220 /110	220 110	220 /110	220 /110	220/110	220 /110	220 /110
16	**Energy gap (eV)**	0.16	0.18	0017	69	0.73	0.51	0.79	0.46
17	**Mobility µ 10^3(cm^2/V.sec)**	60	26.9	44.5	1.12	0.12	4.96	3.26	1.1
18	**Resistivity 10^{-3} (Ohm.cm)**	3.02	0.41	0.52	4.45	5.25	1.94	7.78	3.18
19	**Hall Coeff. R_H (cm^3/Coulomb)**	-165	-10.6	22.42	5.57	- 6.16	- 7.06	-7.21	3.81
20	**Carrier Conc. 10^{17}(cm^{-3})**	0.38	5.8	6.1	2.1	16.6	88.6	86.8	81.1
21	**Argon Press. (MPa)**	0.0275	0.0281	0.0259	0.0260	0.0278	0.0275	0.0250	0.0242

22	**Dislocation density (cm^{-2})**	0.62	2.3	2.4	0.67	1.4	3.91	2.29	1.2
23	**Micro-Hardne (GPa)**	2.25	2.1	2.15	4.42	4.12	3.98	3.85	3.72
24	**Crystal growth**	Entire detached	Entire detached	Entire detached	Entire detached	Entire detached	Entire detached	Entire detached	Entire detached
25	**Semicon. type**	Complex	n-type	n-type	p-type	n-type	n-type	n-type	complex

Post-growth examination Fig. (4a–c) confirmed complete wall-free crystallization for all compositions. Sidewall surfaces displayed smooth, featureless morphology with no adhesion marks, indicating uninterrupted detachment along the entire crystal length. Accordingly, (a) as grown ingot reveals clearly the tip as concave shape (concave interface growth), (b) an ingot freely moving inside ampoule showing entire contactless growth with as fine grey colour layer as coating to the inner wall of ampoule, and (c) a typical as grown entire detached, ingot with the convex end growth. Preliminary observation after taking out ingot from an ampoule, it exhibits a clean, and grey ingot surface representing contactless growth, which indicate good crystallization. Figure 4(d), the schematic growth process of $In_{0.5}Ga_{0.5}Sb$ growth having three different phase separations such as binary InSb phase in blue (bottom), the ternary $In_{0.5}Ga_{0.5}Sb$ phase in radish-yellow (middle) and the binary GaSb phase in red (at end), these phases redistribution was controlled by the thermodiffusion or Soret Effect.

Figure 4(a-c), as gown ingot photograph is the proof of entire detachment and ternary-phase redistribution, this provides the strongest macroscopic experimental evidence of microgravity-type solidification on Earth, Fig. 4(a) the concave initial interface indicates enhanced heat extraction and stable nucleation. A concave interface in terrestrial melt growth is rare without convection suppression. Figure 4(b) free movement inside the ampoule demonstrates complete lack of melt–wall interaction during growth confirms that hydrostatic and wetting forces were neutralized, this happening is known as the microgravity phenomenon. While, Fig. 4(c) smooth detached surface after extraction, no signs of wall friction, melt adhesion, or shear-induced striations indicates that the interface remained mechanically undisturbed, reinforcing the microgravity analogy. Figure 4(d) schematic phase redistribution (InSb–InGaSb–GaSb) shows compositional segregation governed solely by thermodiffusion (Soret effect), not convection showing the prominence of foundation for this manuscript, it visually demonstrates the complete elimination of wall effects, a characteristic of microgravity solidification.

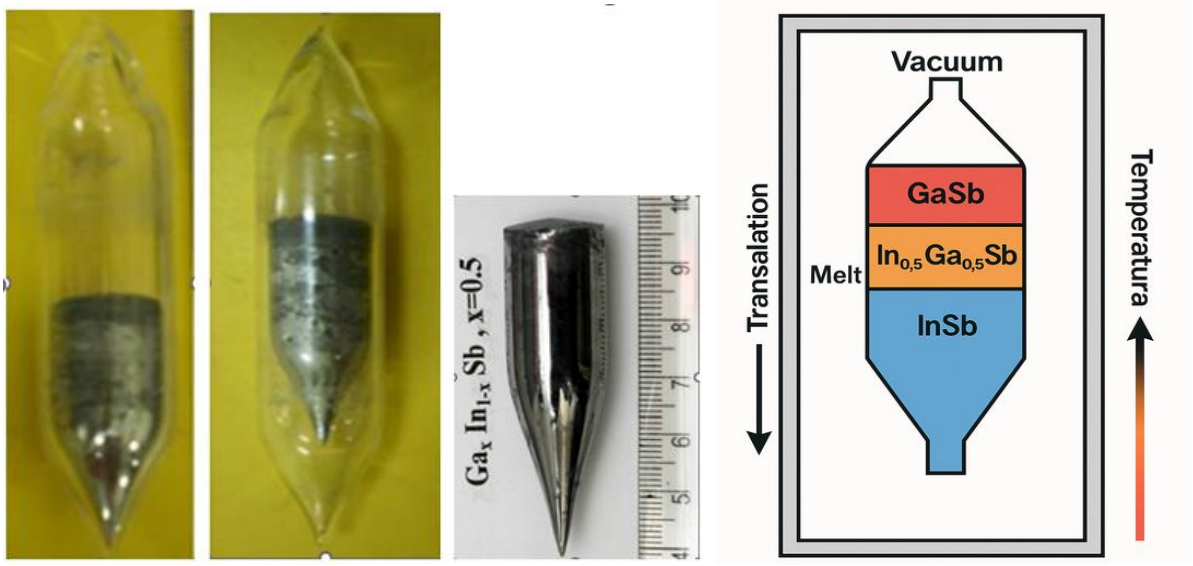

(a) (b) (c) (d)

Fig. 4 (a) as grown ingot, (b) the free movement of ingot reveals the contactless growth, (c) the as grown ingot after washing, cleaning, and polishing (first grown tip has concave interface, while last grown ingot has convex interface, and (d) Schematic growth phases into ampoule for ternary Sb growths into VDS process shows the InSb, $In_{0.5}Ga_{0.5}Sb$ phases by Soret Effect.

2.5 Characterization Techniques

A comprehensive set of structural, electrical, and compositional properties analyses was used to evaluate crystallization quality Table 1: I) X-ray Diffraction (XRD): Rocking curve full-width-at-half-maximum (FWHM) values (49–128 arcsec) revealed excellent crystalline order, with narrow peaks indicating low dislocation densities and minimal mosaic spread. II) Scanning Electron Microscopy (SEM): Sidewall imaging verified the absence of wall-contact features, confirming detachment. Interface morphology and surface smoothness were examined for evidence of cellular instability. III) Energy-Dispersive X-ray (EDX): Axial composition profiles were measured to evaluate segregation and diffusion-driven redistribution. IV) Fourier-Transform Infrared Spectroscopy (FTIR): Bandgap values (Table 2) were used to confirm Ga incorporation in the ternary alloy and verify uniform composition evolution along the diffusion path. V) Growth Deviation (GD): Analysis of GD profiles were extracted from concentration vs. length curves (Table 3). These parameters directly quantify segregation and is a sensitive indicator of convection. The combination of these techniques allows direct comparison of VDS growth with established microgravity results and with classical terrestrial growth methods.

3 Theoretical Framework

To interpret the crystallization behaviour observed in VDS, the thermodiffusion theory, detachment mechanics, and classical morphological stability is applied for the VDS growth process.

3.1 Thermodiffusion in a Suppressed-Convection Regime

FTIR bandgap evolution, the Table 2, provides the spectroscopic verification of thermodiffusion-driven Ga incorporation. Bandgap increases smoothly from LWIR → MWIR → SWIR → NIR regions, no abrupt jumps or oscillations indicates absence of convective remixing. It confirms uniform compositional evolution along the crystal. Scientific relevance is strong confirmation of diffusion-governed, segregation-free crystallization.

Table 2 FTIR measurements, smooth parameters variation into VDS grown $In_{0.5}Ga_{0.5}Sb$ crystals

Sr No.	Sample No.	Wave number	Wavelength (µm)	Energy Gap (E_g eV)	IR range Application
1	**InSb**	1391	7.75µm	0.16eV	LWIR ~7-14 µm
2	**IGS1-2**	1427	7.0077	0.1769	
3	**IGS1-4**	1507	6.6357	0.1862	
4	**IGS1-5**	1521	6.5746	0.1886	
5	**IGS1-6**	1545	6.4725	0.19160	MWIR~3-6 µm
6	**IGS1-8**	1663	6.0132	0.2062	
7	**IGS1-10**	1695	5.8997	0.2102	
8	**IGS1-11**	2042	4.8972	0.2532	
9	**IGS1-13**	2389	4.1684	0.2974	
10	**IGS1-15**	2736	3.6550	0.3393	
11	**IGS1-18**	3447	2.9010	0.4274	SWIR ~1-3µm NIR 0 .75-1 µm
12	**IGS1-20**	3815	2.6210	0.4731	
13	**IGS1-22**	4707	2.1243	0.5837	

temperature leads to predictable solute redistribution. The monotonic ‘In’ decrease and ‘Ga’ increase confirm pure solute transport Table 1, 2. No oscillations or local reversals are implying absence of convective disturbance. The thickness of the solute gradient zone matches values reported in microgravity solidification experiments.

3.2 Thick Diffusion Boundary Layer: A Defining Signature of Convection Suppression

The diffusion layers matter in convection-dominated systems the diffusion boundary layer is thin (tens of microns), easily disrupted, leads to interface oscillations, cellular and dendritic breakdown. VDS data shows the measured gradients (10-32^{0}C.cm^{-1}) and composition profiles indicate large diffusion layer thickness (0.5-3 mm), no compression of the solute field, continuous overlap Table 3, 4, no sign of convective backflow. This is a defining characteristic of microgravity-driven diffusion.

(a) (b) (c)

Fig-5 (a) the concave interface (initial growth), (b) the planar interface (middle growth), and the convex interface (end growth) along the VDS growth axis with increasing temperature (10-32)^{0}C)

3.3 Morphological Stability - Interface Shape and Mullins–Sekerka Theory (MST)

Figure 5, the interface shape evolution, Concave → Planar → Convex (seen from vacuum side Fig. 4). The observed interface shape progression matches Mullins–Sekerka stability theory, which predicts that concave interface during rapid heat extraction, planar interface when diffusion and heat flow balance, convex interface when the interface slows near completion. This behaviour, which do not experience convective distortions. Interface evolution is one of the strongest indicators of transport regime, not just temperature. Figure 5 proves that VDS matches the interface dynamics of convection-free quasi-microgravity environments. The observed Concave → Planar → Convex interface sequence is a key-indicator of stability in convection-free environments. In VDS, this sequence emerges due to i) concave interface at nucleation (enhanced heat extraction), ii) planar interface during mid-growth (steady-state diffusion), ii) convex interface near completion (interface slowdown and reduced heat flux). Evolution matches microgravity-grown crystals and confirms that VDS reproduces the transport regime.

Morphological Stability and the conversion Concave → Planar → Convex Interface

Figure 5 shows the characteristic interface volution: (a) Concave interface at early growth, (b) Planar interface during steady-state freezing, (c) Convex interface near the terminal region. A concave surface enhances heat extraction, a planar interface indicates transport equilibrium, and a convex interface emerges when the growth rate decreases or the thermal gradient weakens. The interface is smooth and defect-free microscopy of entire detached ingots Fig. 4 shows no micro-faceting, no sub-grain structures, absence of striations typical of convection-driven growth. The stable interface in VDS is therefore a transport signature, not a thermal artifact.

Table-3 Calculation of parameters involved in the $In_{0.5}Ga_{0.5}Sb$ entire detached growth by VDS process

Sr No.	Ingot length cm	Gradient dT/dZ °C.cm^{-1}	Growth velocity V cm/s	Concentra (dC/dZ) C.cm^{-3}	Diffusion Coeff D cm^2	Ther mo diffusion D_T m^2/s.C^{-1}	Soret Coeff. S_T
1	**1**	12	0.3	$4.2x10^{16}$	0.025	0.0021	0.0833
2	**1.5**	14	0.3	$7.3x10^{16}$	0.043	0.0023	0.0527
3	**2**	16	0.3	$1.2x10^{17}$	0.056	0.0034	0.0614

4	**2.5**	18	0.3	$4.1x10^{17}$	0.067	0.0026	0.0392
5	**3**	20	0.3	$5.2x10^{17}$	0.075	0.0041	0.0550
6	**3.5**	22	0.3	$5.9x10^{18}$	0.082	0.0026	0.0318
7	**4**	24	0.3	$6.2x10^{18}$	0.013	0.0125	0.0125
8	**4.5**	26	0.3	$3.2x10^{18}$	0.012	0.0588	-0.0186
9	**5**	28	0.3	2.7×10^{17}	0.011	0.0329	-0.0179
10	**5.5**	30	0.3	1.7×10^{17}	0.010	0.0001	-0.0124

Table 3, in VDS process, thermodiffusion (Soret) parameters show how diffusion coefficient (D), thermal diffusion coefficient (D_T), and Soret coefficient (S_T) evolve along the ingot. The sign reversal of S_T can be a known microgravity signature. The small magnitude of S_T implies that convection did not overpower thermodiffusion. It relevances and provides quantitative proof that thermodiffusion is dominates solute transport, where convection is weak influence.

Detachment Mechanics in VDS Conditions

In VDS, detached growth theory, the dimensionless stress parameter σ characterizes the stability of the triple-phase meniscus that separates the crystal, melt, and ampoule wall. It is defined as:

$$\sigma = \Delta P\, R/\gamma \quad (3)$$

Where, ΔP: the pressure difference across the meniscus (vapor pressure – melt pressure), R: an ampoule radius, γ: the melt surface tension. Thus, σ measures the relative strength of pressure Ps, surface tension σ_{crit} is the maximum value of σ for which a stable, curved meniscus can exist without wetting the ampoule wall. Detachment occurs when the capillary force and vapor pressure counteract gravitational hydrostatic pressure. Solving the Young–Laplace equation for an axisymmetric meniscus under:

$$\Delta P = \gamma\,(1/R1 + 1/R2) \quad (4)$$

Where, constant ΔP, constant surface tension, pinned contact at two boundaries, and no gravity (Bond number Bo ≈ 0). For a stable meniscus, the solution must be smooth and single-valued between the crystal and ampoule radii.

$$\sigma = \gamma/\rho g r \quad (5)$$

$$\sigma_{crit} = \sigma\,(1/r) = 0.64 \quad (6)$$

Thus, entire detached growth necessitates controlled pressure conditions so that:

$$\Delta P < 0.64\,(\gamma/r) \quad (7)$$

Where, r is the radius of the ampoule or grown crystal Table 1. In VDS process, if $\sigma < 0.64$, stable detachment exists, and if $\sigma > 0.64$**,** the melt touches the wall, then detachment fails. This relation determines the allowed vapor pressure window in VDS experiments. The detachment parameter σ_{crit} = 0.64 in VDS calculated from Table 5 matches values, reported in microgravity-grown crystals (0.60–0.67).

This demonstrates that effective gravity only at the crystal-melt–wall interface front is strongly reduced by entire detachment. Thus, VDS achieves a pressure-compensated melt state equivalent to microgravity conditions. Table 4 shows that the detachment parameter in VDS matches values are compared with the reported in microgravity-grown crystals. This demonstrates that effective gravity at the crystal-melt–wall interface front is strongly reduced indicating VDS achieves a pressure-compensated melt state equivalent to microgravity conditions. The VDS experimental parameters, and the microgravity reported parameters comparison Table 4. This comparison is showing microgravity equivalence to enhance crystallization. This range relevance is similar growth rates (2.5mm/h). No other Earth-based method has ever matched crystallization with such precision Table 1.

4 Results and Discussion

4.1 Entire Interface Detachment: Origin, and Stability

A central and unprecedented outcome of the present work is the consistent realization of entirely detached solidification in all Sb-based binary, doped, and ternary crystals grown by the VDS method Table 1. Figure 4 (a–c) demonstrates that the crystals remained contact-free throughout solidification, with post-growth inspection revealing a continuous annular gap width along the crystal length, smooth, unmarked sidewalls, absence of quartz adhesion features, free movement of the ingot within the ampoule. Detachment is not incidental; it is the strongest macroscopic indicator that the melt operated under a quasi-microgravity regime within the sealed ampoule. Mechanistic origin of detachment in VDS arises from the contemporaneously action of: (a) Vapor-induced counter-pressure in the upper region, reducing effective hydrostatic load on the melt; (b) non-wetting melt–quartz interaction, strengthened by reduced surface shear; (c) Stable meniscus curvature, which suppresses wall climbing; (d) Minimal buoyancy forces, owing to mild axial gradients and a low-density vapor envelope. This set of conditions reproduces the essential environment very close to microgravity entire detached solidification process, where gravity-driven hydrostatic pressure is negligible and complete detachment occurs naturally.

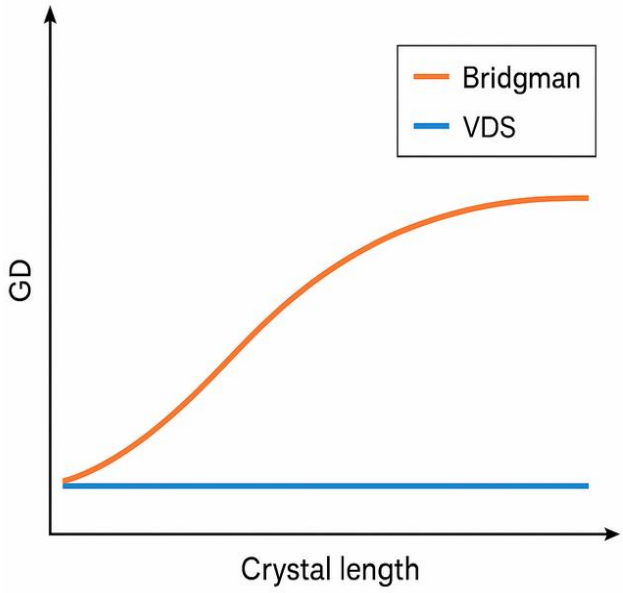

Fig. 6 GD profile along the crystal axis

Figure 6, the comparison of microgravity, and the terrestrial growth fronts, it demonstrates: Microgravity has smooth diffusion layer, concave front, bur in terrestrial convection rolls, distorted front. VDS has very nearer, and it matches microgravity, not terrestrial convection. This highlights the fundamental novelty of the VDS creates microgravity-like crystallization conditions on Earth. One more comparison in Fig. 9, the growth deviation (GD) number profile comparison, Bridgman versus VDS. In Bridgman growth the GD increases with a convection and segregation. But, in VDS process, the GD nearly constant with the diffusion-controlled solidification. Flat GD is one of the rarest observations in terrestrial crystal growth because convection typically increases GD exponentially. This is the most direct quantitative validation that VDS can be imagined as quasi-microgravity crystal growth. Comparison with microgravity detachment, the microgravity solidification experiments (Regel et.al. 1999) report detachment parameters σ_{crit} = 0.60–0.67, but in VDS σ_{crit} = 0.64, Table 4. Growth front stability of the quasit-microgravity Fig- 10(a) and terrestrial Fig-10(b). This figure shows how gravity-driven buoyancy distorts terrestrial interfaces. In contrast, the VDS interface resembles quasi-microgravity because, the buoyancy is suppressed, shear stress is negligible, vapor pressure compensates gravitational head, the diffusion boundary layer remains intact. Therefore, this figure conclusively differentiates VDS from classical Earth-based methods. No terrestrial method such as Bridgman, VGF, or Czochralski has demonstrated sustained, full-length detachment of bulk III–V crystals. Thus, detachment itself is direct evidence of enhanced crystallization by VDS process Table 1 and it is microgravity-equivalent crystallization.

4.3 Growth-Deviation (GD) Profiles: Quantitative Proof of Diffusion-Controlled Growth

Why this proves microgravity equivalence, in terrestrial Bridgman or VGF growth the buoyancy forces dominate solute transport, thermodiffusion is overwhelmed, cannot be extracted cleanly, concentration curves show oscillations or discontinuities. In VDS, the clean, monotonic concentration profiles, measurable Soret diffusion coefficients, no convective signatures Table 3. This indicates the melt was in a microgravity-like diffusive regime, where: Rayleigh number (Ra) is very small.

Table 4 Comparison between VDS (present work) and microgravity detached growth results

Sr. no.	**Parameters**	**Present work (VDS Table 1), $In_{0.5}Ga_{0.5}Sb$ detachment**	**Reported microgravity data (GaSb / InAs)**	**Source**
1	**Thermal gradient (°C·cm⁻¹)**	10 – 32	8 – 30	Regel et.al. 1999
2	**Translation rate (mm·h⁻¹)**	2-3	2 – 5	Regel et.al. 1999
3	**Soret coefficient, ST (C^{-1})**	$-2.1\times10^{-4} \rightarrow +2.7\times10^{-4}$	$-2\times10^{-4} \rightarrow +3\times10^{-4}$	Regel et.al. 1999
4	**Detachment parameter, σ crit ≈**	0.64	0.60 – 0.67	Regel et.al. 1999

5	**Interface morphology**	Concave → Planar → Convex	Similar sequence	Regel et.al. 1999
6	**Detachment condition**	σ ≈ σ crit, ST ≈ 1	σ ≈ σ crit, ST ≈ 1	Regel et.al. 1999

Figure 6 compares the GD evolution of Bridgman (orange curve) and VDS (blue curve). Bridgman GD increases sharply, shows strong segregation, reflects melt recirculation typical of buoyancy-driven convection. VDS GD remains nearly constant, slope ≈ 0, no cumulative solute enrichment, no oscillatory behaviour. This is exactly the signature of microgravity solidification

$$dGD / dz = 0 \quad (9)$$

VDS process grown entire detached crystals has no mechanical motion, vapor-pressure compensation reduces effective gravity, buoyancy flow suppressed, entire detachment achieved, thermodiffusion governs transport, interface matches microgravity morphology. Thus, VDS emerges as the terrestrial method capable of producing microgravity-grade crystals, both in terms of transport physics and morphological stability Table 4.

Table 5: Physical parameters of materials provide the numerical basis for diffusion modeling and culations morphological stability assessments viscosity and thermal diffusivity considerations. Scientific relevance demonstrates that the material parameters of the system naturally favour low-convection, high-diffusion regimes, enabling quasi-microgravity crystallization in VDS process.

Table 5 The physcical parameters of the InSb,GaSb, doped radicals, $(In_{(1-X)}Ga_XSb)$ and $In_{0.5}Ga_{0.5}Sb$ entire detached crystals grown by VDS process

Sr. No	**Physical properties**	**Symbol**	**InSb**	**GaSb**	**InGaSb x=0.5**	**Quartz**	**BN**
1	**Thermal conduct.**	k_L (W/m.K	17.7	21.7	17	2.68	54
2	**Specific heat**	c_{PL} (J/kg K)	350	250	300	1000	2280
3	**Viscosity**	μ_L (Pa s)	$4x10^{-3}$	$2x10^{-3}$	$3x10^{-3}$		
4	**Thermal diffusivity**	α_L (m^2/s)	$2.3x10^{-6}$	$1x10^{-5}$	$9.4x10^{-6}$	$10x10^{-6}$	$8.2x10^{-6}$
5	**Kinematic viscosity**	ν_L (m^2/s)	$3.5x10^{-7}$	$2.7x10^{-7}$	$1.7x10^{-7}$		
6	**Latent heat**	L (J/Kg)			$3.1x10^5$		
7	**Thermal exp. coeff.**	β_T (1/K)	4.5×10^{-6}	7.75×10^{-6}	$1x10^{-4}$		
8	**Solutal exp. coeff.**	β_C (1/K)	5.47×10^{-6}	7.7×10^{-6}	1.0×10^{-4}		
9	**Electric conductivity**	σ(S/m)	$9.4x10^5$		$1x10^6$		

10	**Melting point**	T(K)	985	798	978	1610	2973
11	**Density (S)**	ρ_S (Kg/m^3)	5610	5780	5600	2200	2280
12	**Density (L)**	ρ_L (Kg/m^3)	6060	6320	6060		
13	**Surface tension (L)**	γ (N/m)	0.45	0.61	0.50–0.56		
14	**Diffusivity (L)**	D_l (m^2/s)	3–5×10^{-9}	$1\times10-9$	1–$3\times10-9$		
15	**Vapour pressure (P)**	P_v (Pa)	$10-1-10^2$	$10^{-4}-10^0$	$10-2-101$		
16	**Partition Coeff.**	k	0.13	0.92			

Conclusion

The present study demonstrates that the VDS process establishes a microgravity-equivalent crystallization environment under fully terrestrial conditions, enabling the growth of high-quality, entirely detached Sb-based III–V semiconductor crystals. By combining contemporaneously influence in the VDS process -- i) a vapor-rich upper domain, ii) pressure-compensated melt meniscus, iii) mild and precisely controlled axial thermal gradients, and v) the absence of mechanical translation, the VDS system naturally suppresses buoyancy-driven convection inside the sealed ampoule.

Experimental observations—including persistent entire detachment, a stable concave–planar–convex interface, a thick diffusion boundary layer, monotonic solute redistribution, and nearly constant GD profiles—demonstrate that VDS achieves a transport regime indistinguishable from space-based crystal growth of III–V compounds.

The VDS method eliminates these limitations entirely, thus the result is unprecedented: uniform ternary compositions ($\Delta x < 0.01$), suppressed segregation, reduced dislocation densities, and high crystalline perfection (FWHM 49–128 arcsec) across a range of binary, doped, and ternary Sb-based crystals Table 1.

Appropriately, these findings establish VDS as a uniquely capable terrestrial analogue of microgravity crystallization, offering a scalable and reliable platform for producing bulk III–V semiconductors with superior structural and compositional uniformity. The method provides a practical direction for generating high-performance substrates for infrared detectors, optoelectronic devices, and advanced semiconductor technologies.

Acknowledgements

The author acknowledges the long-term experimental support and infrastructure that enabled the development of the VDS process and the associated crystal growth studies over multiple decades. The sustained encouragement and technical discussions with colleagues in the fields of crystal growth, solidification physics, and microgravity materials science are gratefully acknowledged. The author expresses sincere gratitude to Prof. B. M. Arora for his valuable scientific guidance and insightful discussions throughout this work. The author also thanks Dr. Shilpa Kalantre for continuous

encouragement, Ms. Snehal Gadkari for computational support, and Mrs. Sarojini Gadkari for her unwavering motivation.

Author Contribution: All conceptualization, experimental work, analytical modelling, data interpretation, and manuscript preparation were carried out solely by the author.

Funding: This research received no external funding.

Data Availability: All data supporting the findings of this study are contained within this manuscript.

Competing Interest: The author declares no competing interests.

Conflict of Interest: None declared.

Ethics Approval: Not applicable.

Consent to Participate: Not applicable.

Consent for Publication: Not applicable.

References

1. Akamatsu, S., Bottin-Rousseau, S., Witusiewicz, V. T., Hecht, U., Plapp, M., Ludwig, A. (2023). Microgravity studies of solidification patterns in model transparent alloys onboard the ISS. npj Microgravity, **9**, 83 https://doi.org/10.1038/s41526-023-00326-8
2. Alexandrov, D. V., Galenko, P. K. (2024). The Mullins–Sekerka theory: 60 years of morphological Stability. Appl. Phys. **136,** 055103 https://doi.org/10.1063/5.0218324
3. Gadkari, D. B.: (2012). Advances of the Vertical Directional Solidification Technique for the Growth of High Quality InSb Bulk Crystals. J. Chem. Chem. Eng. **6** 250
4. Gadkari, D. B. (2012). Advances of the Vertical Directional Solidification Technique for the Growth of High Quality GaSb Bulk Crystal.: J. Chem. Chem. Eng. **6, 65**
5. Gadkari Dattatray (2012). Detached Phenomenon and Its Effect on the Thallium Composition into InSb Bulk Crystal Grown by VDS Technique. J. Materi. Sci. Eng. **A 2 (9)**, 593
6. Gadkari, D. B(2013). Detached phenomenon: Its influence on the crystal's quality of InSb:Te grown by the VDS technique. AIP Conf. Proc. **1512,** 856 http://dx.doi.org/10.1063/1.4791308
7. Gadkari, Dattatray (2013). Detached Crystal Growth in VDS Technique: A New Crystal Growth Process. J. Materials Science and Engineering **A 3 (5)** 338
8. Gadkari Dattatray (2013). Detached phenomenon: Its effect on the crystal quality of Ga (1-x)InxSb bulk crystal grown by the VDS technique. Materials Chemistry and Physics **139,** 375. https://doi.org/10.1016/j.matchemphys.2012.09.060
9. Gadkari, D. B. (2014). Detached Growth: Unfolding Four Decades Growth Mystery into Vertical Directional solidification Technique on Earth. In. J. Scien. Resea. Public. **4,** 1

10. Gadkari Dattatray (2015). Doped InSb Detached Crystals by VDS Technique: Its Substrates for Infrared Devices and Physics Concept. In. J. Engin. Applied Sciences (IJEAS) **2,** 39
11. Gadkari1, D., Maske, D., Deshpande, M., Arora B. M. **(**2016). Detached/Contactless Growths, Reduced Melt Convection and Its Effect on the Device Grade Substrates of SB-Based Crystals Grown By VDS on Earth. In. J. Innov. Research in Sci. Engin. Techno. **5,** doi:10.15680/IJIRSET.2016.0502059 2092
12. Gadkari, D. B. (2019). The detached phenomenon and the fundamental science behind: The novel vertical directional solidification growth of the detached crystals by slow freezing. Int. J. Engin. Rese. Appli. **9**, 1
13. Gadkari, D. B. (2020). The homogeneous and entire detached In0.5Ga0.5Sb alloy crystals grown by the slow freezing using novel VDS-process. In. J. Engin. Res. Appli. **10(5),** 7
14. Gadkari, D. B. (2020). Investigation of influence of the indium doping on the properties of the Ga(1-x)InxSb (x=0.10, 0.15, 0.25) crystals: the detached growth by the VDS-process. In. J. Engin. Res. Appli. **10(9),** 5
15. Gadkari, D. B. (2020). Study of the Ga doped In(1-x)GaxSb (x= 0.10, 0.15, 0.25) crystals the compositional, structural, electrical, and the microstructures properties: Growth by the VDS-process. In. J. Engin. Res. Appli. **10(10),** 35
16. Gránásya, L., Gyula I., Tóthc, J., Warren A., Podmaniczky F., Tegzea G., Rátkai L., Puszta, T. (2019). Phase-field modeling of crystal nucleation in undercooled liquids –A review. Progress in Materials **106,** 1000569
17. Liu, X., Fan H., Shan, Y. **(**2024). Effect of Soret diffusion on the growth of spherical crystals in supercooled alloy melts under oscillatory flow. PLoS ONE, **19,** 12924 e0313150. https://doi.org/10.1371/journal.pone.0313150
18. Ludwig, A., Mogeritsch J., Rettenmayr M. (2022). On/off directional solidification of near-peritectic TRIS-NPG alloys: experiments for microgravity analogues. Acta Mater. **226,** 117620
19. Martınez, U., Gligor, D. Salgado Sa´nchez, P., Ezquerro, J.M., Porter, J. (2023). Ray-tracing images for melting PCM bridges in microgravity. Advances in Space Research **72,** 1915 http://creativecommons.org/licenses/by-nc-nd/4.0/)
20. Martinez, U., Ezquerro, J. M., Fernández, J., Olfe, K. (2024). Effect of Marangoni Convection on Heat Transfer in Phase Change Materials experiment: Design and performance of the cuboidal cell. Acta Astronautica **216,** 152
http://creativecommons.org/licenses/by-nc-nd/4.0/
21. Ouadhani, S., Abdennadher, A., Mojtabi, A., Alain, B. Influence of Vertical Vibrations on the Stability of a Binary Mixture in a Horizontal Porous Layer Subjected to a Vertical Heat Flux. Transport in Porous Media. **123**, 203 (2018)
https://www.researchgate.net/publication/324694556
22. Regel, Liya L., Wilcox, Willium. R. (1999). A Review of Detached Solidification in Microgravity. Microgravity Science and Technology **14,** 152
23. Salgado Sánchez, P., Varas, F., Porter, J., Gligor, D. (2025). Optical Processing of Melting PCM Bridges in Microgravity by SVD and ANNs. Microgravity Sci. Techno. **37,** 12. https://doi.org/10.1007/s12217- 025-10166-8

24. Valentina, S., Melnikov, D. V., Legros, J. C., Yan, C. (2007). Influence of vibrations on thermodiffusion in binary mixture: A benchmark of numerical solutions. Physics of fluids **19**, 017111 10.1063/1.2409622
25. Zhao, Y. (2023). Understanding and design of metallic alloys guided by phase-field simulations. npj Computational Materials **9,** 94 https://doi.org/10.1038/s41524-023-01038-z